Environmental Science & Technology

Article

pubs.acs.org/est

Analyses of Turbulent Flow Fields and Aerosol Dynamics of Diesel Engine Exhaust Inside Two Dilution Sampling Tunnels Using the CTAG Model

Yan Jason Wang,[†] Bo Yang,[‡] Eric M. Lipsky,[§] Allen L. Robinson,[∥] and K. Max Zhang*[,†]

[†]Sibley School of Mechanical and Aerospace Engineering, Cornell University, Ithaca, New York, United States

[‡]College of Automotive Engineering, Jilin University, Changchun, China

[§]Engineering, Pennsylvania State University Greater Allegheny, McKeesport, Pennsylvania, United States

[∥]Department of Mechanical Engineering, Carnegie Mellon University, Pittsburgh, Pennsylvania, United States

Supporting Information

ABSTRACT: Experimental results from laboratory emission testing have indicated that particulate emission measurements are sensitive to the dilution process of exhaust using fabricated dilution systems. In this paper, we first categorize the dilution parameters into two groups: (1) aerodynamics (e.g., mixing types, mixing enhancers, dilution ratios, residence time); and (2) mixture properties (e.g., temperature, relative humidity, particle size distributions of both raw exhaust and dilution gas). Then we employ the Comprehensive Turbulent Aerosol Dynamics and Gas Chemistry (CTAG) model to investigate the effects of those parameters on a set of particulate emission measurements comparing two dilution tunnels, i.e., a T-mixing lab dilution tunnel and a portable field dilution tunnel with a type of coaxial mixing. The turbulent flow fields and aerosol dynamics of particles are simulated inside two dilution tunnels. Particle size distributions under various dilution conditions predicted by CTAG are evaluated against the experimental data. It is found that in the area adjacent to the injection of exhaust, turbulence plays a crucial role in mixing the exhaust with the dilution air, and the strength of nucleation dominates the level of particle number concentrations. Further downstream, nucleation terminates and the growth of particles by condensation and coagulation continues. Sensitivity studies reveal that a potential unifying parameter for aerodynamics, i.e., the dilution rate of exhaust, plays an important role in new particle formation. The T-mixing lab tunnel tends to favor the nucleation due to a larger dilution rate of the exhaust than the coaxial mixing field tunnel. Our study indicates that numerical simulation tools can be potentially utilized to develop strategies to reduce the uncertainties associated with dilution samplings of emission sources.

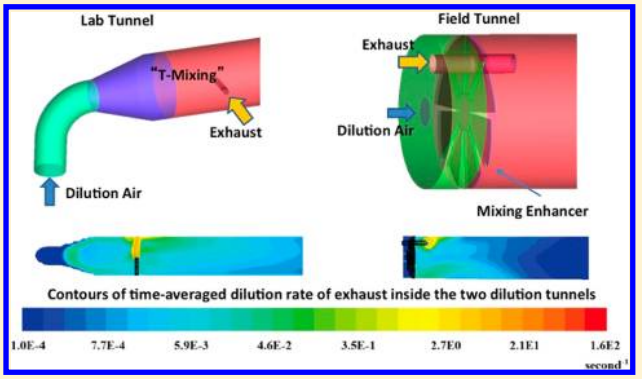

1. INTRODUCTION

The development of emission inventories and regulations relies on the results from emission testing.[1,2] Because of its high temperature and high concentrations, the raw exhaust from combustion sources needs to be diluted for speciation and quantification, especially for its particulate components.[1,3,4] Therefore, fabricated dilution systems are essential to almost all emission testing procedures and major combustion sources (e.g., diesel engines, gas turbines, biomass stoves).[2−4]

Dilution systems have been utilized for various purposes: (1) to capture the atmospheric dilution, especially for establishing a link between the atmospheric dilution and the undiluted exhaust;[5,6] and (2) to preserve the exhaust properties as unbiased as possible from the measurement and dilution setup artifacts to produce a so-called "tailpipe-level" emissions as observed inside the exhaust pipe.[7] For either purpose, the current dilution samplings have many known limitations and those limitations are pronounced for measuring the semivolatile composition and the ultrafine range (<100 nm) of the particulate emissions. Dilution air properties have been shown to have a strong influence on particle size distributions. One can obtain up to 2 orders of magnitude change in ultrafine particle (UFP) concentrations from an engine operating at a steady state condition by changing dilution air properties.[8,9] Nucleation-mode particles, typically originated from sulfuric acid−water nucleation followed by condensational growth of organic carbons, are found to be sensitive to sampling conditions and thus the laboratory measurements may differ considerably from on-road emissions depending on chosen dilution parameters.[6,10]

Received: June 25, 2012
Revised: November 23, 2012
Accepted: November 28, 2012
Published: November 28, 2012

Table 1. Dilution Parameters Controlling the Emission Measurement of Combustion Sources

Group I. Aerodynamics	
Fixed parameters (i.e., dilution tunnel configuration)	Mixing type of the dilution tunnel: T-mixing dilution tunnel,[2,4] coaxial mixing dilution tunnel,[2] perforated tube diluter (Dekati Ltd.), ejector diluter (Dekati Ltd.), rotating disk diluter (Matter Engineering Inc.), etc.
	Mixing enhancer: fan shape plate,[2] orifice plate, baffle, etc.
Variable parameters (i.e., operating conditions)	Dilution ratio (DR) at the end of the dilution tunnel
	Residence time inside the dilution tunnel
Group II. Mixture properties	
Properties of engine exhaust: temperature, water content, sulfuric acid concentration, OC concentration and composition, size distribution of the primary soot-mode particles, etc.	
Properties of dilution gas: temperature of dilution gas, relative humidity (RH), particle size distribution, OC concentration and composition, type of dilution gas (e.g., pure nitrogen or air), etc.	

In recent years, numerical methods have been utilized to improve our understanding of the flow field and aerosol dynamics inside the fabricated dilution systems.[11−13] Vouitsis et al.[13] applied a box model of nucleation, condensation, coagulation, and diffusional losses to the walls in a porous dilutor, assuming that the mixing of exhaust within the dilutor occurs instantaneously. One challenge regarding the dilution process of exhaust is that the majority of dilution tunnels are operated under a turbulent condition. Therefore, it is important to understand the turbulence and its effect on aerosol dynamics inside the dilution tunnels, especially those with complex geometries. Under this circumstance, a computational fluid dynamics (CFD) model has been employed to simulate the nucleation of dibutylphthalate in a perforated tube diluter.[12]

Previously, we have evaluated the Comprehensive Turbulent Aerosol Dynamics and Gas Chemistry (CTAG), a CFD-based turbulent reacting flow model, in resolving vehicle-induced turbulence and aerosol dynamics of individual plumes in the atmosphere.[14] In this paper, we employ CTAG to investigate the dilution processes of the same diesel exhaust inside two dilution tunnels. We aim to answer the following questions: (1) How do the turbulent mixing processes in the two dilutors differ from each other? and (2) How does the turbulent mixing process interact with aerosol dynamics that affects particulate emission measurements? Future studies will compare the turbulent mixing processes inside the dilution systems with those in the atmosphere.

2. DILUTION PARAMETERS CONTROLLING THE EMISSION MEASUREMENT OF COMBUSTION SOURCES

Studies have shown that various design and operation parameters can affect the functionality of dilution tunnels.[1,2,11,15,16] We separate them into two groups based on their characteristics, as described in Table 1, which provides the background for the follow-up discussions and potentially the guideline for future designs.

The tunnel configuration in Group I ("Aerodynamics") is usually designed ahead of the measurements and remains fixed during the measurements, while the operating conditions can vary during the experiment depending on the purpose of the study.

For Group II ("Mixture Properties"), the properties of exhaust (e.g., temperature, sulfuric acid concentration) depend on the types of fuel, engines, after-treatment devices, and their operating conditions during the experiment,[17] while the properties of dilution gas (e.g., relative humidity and temperature) can be varied during the experiment depending on the purpose of the study.[16,18]

In summary, these dilution parameters contribute to the complexity of the design and operation of dilution tunnels. Therefore, a thorough understanding of their individual effects as well as coupled effects is necessary. In this study, we focus on selected parameters in the two groups inside a single stage dilution tunnel, while some experiments had two or more stages of the dilution systems combined to achieve the desired dilution ratios (DR).[6,10]

3. EXPERIMENTAL SECTION

Experiments were conducted to compare the performance of a portable field dilution tunnel, noted as "field tunnel", with a larger dilution tunnel primarily used in laboratories, noted as "lab tunnel".[2] The emission source was provided by a single-cylinder Yanmar L70AE air-cooled diesel engine and tests were conducted at a low load (25% of full capacity). The intercomparison experiments involved simultaneous sampling with the two dilution tunnels from the same location of an enclosed exhaust duct. Therefore this experiment setup eliminates the difference in exhaust properties, and focuses on the effect of the dilution process on particle number concentration measurements. Particle size distributions (PSDs) were measured from 10 to 460 nm using a TSI Scanning Mobility Particle Sizer (TSI 3081 DMA with the model 3010 CPC) through a 120-s up scan and a 30-s down scan. It should be noted that this engine was running under a steady-state condition, which made the comparison between the function of two dilution tunnels more reliable and repeatable under a low sampling response. Potentially, the transient-state condition of diesel engine could be studied in the future to capture the real-world on-road particle emissions with a high sampling response.[19,20]

Figure 1 illustrates the differences in the configurations of lab tunnel and field tunnel, i.e., their aerodynamics-related parameters (i.e., Group I). The main difference is that the lab tunnel employs a T-mixing configuration and the field tunnel utilizes coaxial mixing. Moreover, a fan-shaped mixing enhancer is installed in the field tunnel, but not in the lab tunnel. The two dilution tunnels also vary in length, with the lab tunnel (2.3 m) longer than the field tunnel (0.9 m). But both tunnels have the same diameter. The flow rate through the lab tunnel is ∼1000 Lpm, while the field tunnel is operated at ∼174 Lpm. Therefore both tunnels are maintained at a residence time (RT) of ∼2.5 s.[2] DR is determined by simultaneously measuring CO_2 levels of exhaust and diluted exhaust at the end of the tunnels, as described in the Supporting Information (SI). Experiments under two DRs, 20 (noted as DR20) and 120 (noted as DR120) were conducted for both tunnels.

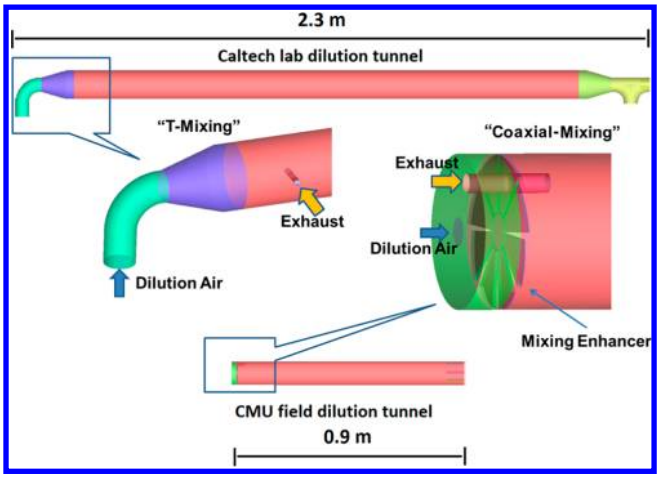

Figure 1. Configurations and computational domains of two dilution tunnels.

4. MODELING METHOD

4.1. CTAG Model. The CTAG model, introduced in Wang and Zhang,[14] is employed to simulate the turbulent flow field and aerosol dynamics within the dilution tunnels. The turbulent flow field inside the dilution tunnel is solved by the Large-eddy Simulation (LES) model,[21] which has demonstrated good ability to capture the flow and mixing features in internal flows when compared to experimental data.[22,23] In current study, multiple aerosol dynamics processes, including nucleation, condensation, evaporation, coagulation, and deposition, are used to capture the evolution of number concentration, size distribution, and chemical composition of multicomponent aerosol particles.[14] We assume that most of the organic carbons reside in the gaseous phase at the exit of the exhaust inlet due to high temperature and the particulate phase only contains combustion-generated soot particles. As temperature cools down, the condensable organic carbons will partition between the gaseous and particulate phases. In addition, the volatility distribution of organic carbons is taken as that derived based the same diesel engine.[33] As discussed in Wang and Zhang, in order to consider the effects of turbulent fluctuations on aerosol dynamics, a presumed finite-mode probability-distribution function (PDF) method[24] is used to couple the turbulent mixing process with the aerosol dynamics and capture the micromixing effects on aerosol dynamics. The aerosol dynamics module and the presumed finite-mode PDF method are written in C-language and incorporated into ANSYS FLUENT through User-Defined Function (UDF).[21] A detailed description of the CTAG model setup can be found in the SI.

4.2. Model Implementation. As shown in Figure 1, the three-dimensional computational domains of the two dilution tunnels are built. They are discretized into approximately 1 million hexahedral cells and shown in the SI Figure S1. Mesh independence studies have been conducted to ensure that the grid resolution is refined for the accuracy of the simulation. A no-slip condition is set to the wall of the dilution tunnels. Boundary conditions for the velocity inlets of diesel exhaust and dilution air under different cases are shown in Table 2. For the outflow condition, a zero normal first derivative of all quantities is fulfilled.

As shown in Table 2, most of the mixing properties, i.e., the Group II parameters, are the same under the four cases, except the RH of the dilution air. For the lab tunnel, the dilution air

Table 2. Boundary Conditions for CTAG Simulations under Different Cases, Obtained from the Experiment

	diesel exhaust					dilution air				
case	exhaust temperature (K)	sulfuric acid mass concentration	exhaust OC mass concentration	exhaust CO_2 mass concentration	UFP concentration (particle cm^{-3})	dilution air temperature (K)	RH of dilution air (@ 297 K)	dilution air CO_2 mass concentration	UFP concentration (particle cm^{-3})	dilution-corrected[a] UFP concentration at the end of tunnels (particle cm^{-3})
1. lab tunnel DR20	514	2.32×10^{-6}	5.52×10^{-5}	0.086	8.52×10^{7}	297	10%	5.80×10^{-4}	7.20×10^{4}	1.54×10^{9}
2. lab tunnel DR120	514	2.32×10^{-6}	5.52×10^{-5}	0.086	8.52×10^{7}	297	<1%	5.80×10^{-4}	7.20×10^{4}	7.93×10^{8}
3. field tunnel DR20	514	2.32×10^{-6}	5.52×10^{-5}	0.086	8.52×10^{7}	297	<1%	5.80×10^{-4}	7.20×10^{4}	7.47×10^{8}
4. field tunnel DR120	514	2.32×10^{-6}	5.52×10^{-5}	0.086	8.52×10^{7}	297	<1%	5.80×10^{-4}	7.20×10^{4}	7.69×10^{8}

[a]PSDs at the end of the tunnel multiplied by their corresponding DRs.

dx.doi.org/10.1021/es302376d | Environ. Sci. Technol. 2013, 47, 889−898

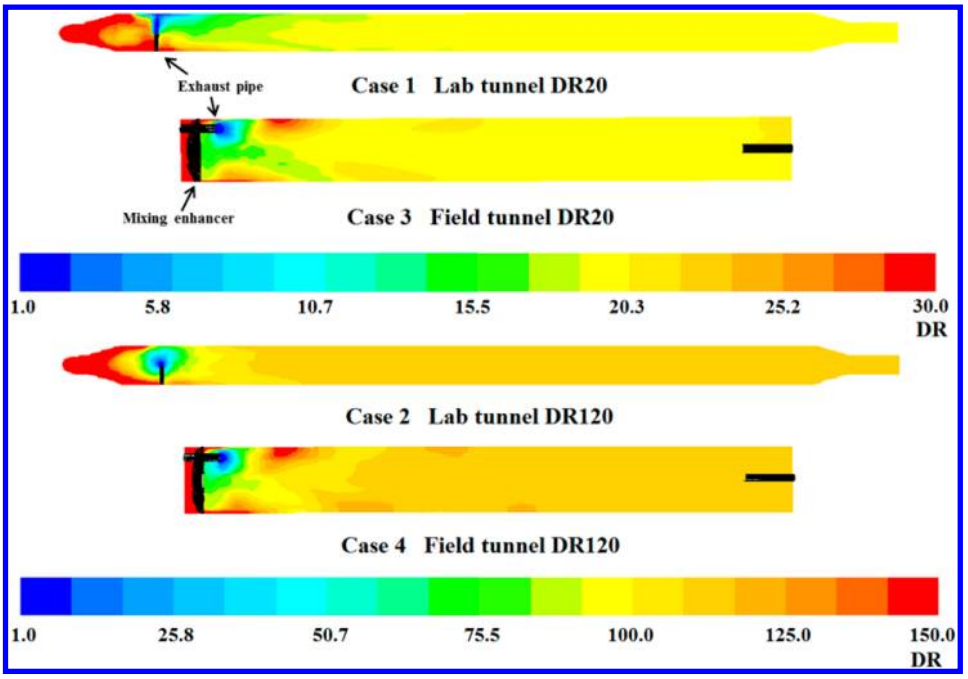

Figure 2. Time-averaged distributions of DR in the cross-section through the exhaust pipe within the two dilution tunnels. Blue represents the exhaust and red represents the dilution air, colors between blue and red represents the degree of dilution. The corresponding instantaneous distributions of DR within the two dilution tunnels are shown in SI Figure S2.

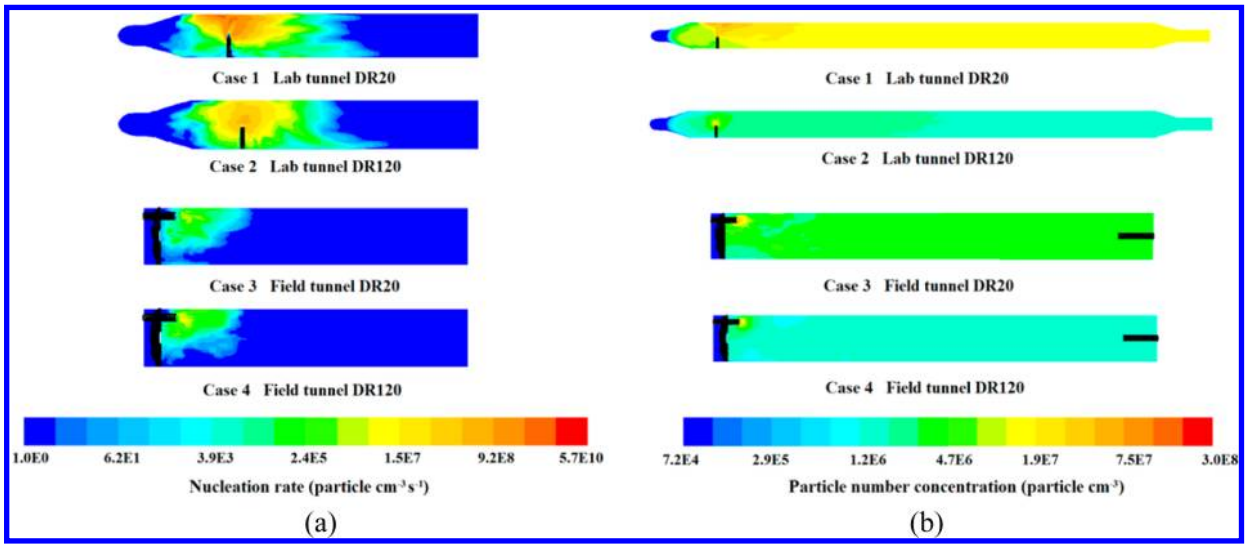

Figure 3. Time-averaged distributions of (a) nucleation rate (near the injection area of exhaust) and (b) the level of UFP concentration inside the two dilution tunnels. The corresponding instantaneous distributions of nucleation rate and UFP concentration within the two dilution tunnels are shown in SI Figures S5 and S6.

used at DR120 (Case 2) is drier than that of DR20 (Case 1), while the RH of the dilution air used in the field tunnel (Case 3 and 4) is also low. The exhaust sulfuric acid mass concentration depends on the fuel sulfur content (FSC), the SO_2-to-SO_3 conversion rate (cr), and the air–fuel ratio. FSC is ~500 ppm for the diesel fuel used in the measurement. A/F is ~32 for the low load. The value of cr depends on several engine operation parameters, e.g., the engine load, and is estimated to be in the range of 4–8%.[13] In this study, the cr value that best matches the predicted and measured particle number concentrations is found to be approximately 5%. More discussion and sensitivity studies regarding cr can be found in Section 5.5 and the SI. The levels of organic carbon (OC) and elemental carbon (EC) were determined by collection on quartz filters and analysis using a Sunset Laboratories Laboratory Thermal-Optical Transmission OC/EC Analyzer.[25] The volatility distribution of OC is described in SI Tables S2 and S3. The size distributions of particles in the dilution air and soot-mode particles in the exhaust are obtained from the experimental measurements. PSD modeled by CTAG is represented by 22 size bins ranging from 1 to 400 nm.

5. RESULTS AND DISCUSSION

5.1. Analysis of Turbulent Flow Fields Inside Two Dilution Tunnels. The dilution process of diesel exhaust inside the dilution tunnel is indicated by the DR, shown in

Figure 2. It can be seen that due to the effect of strong turbulence near the exhaust pipe inlet, the raw exhaust is mixing rapidly with the dilution air, illustrated by the fast transition in colors. The spatial inhomogeneity disappears under turbulent and molecular mixing. For both tunnels, the well-mixed status is achieved before the diluted exhaust reaches the end of the dilution tunnels. The diluted exhaust moves relatively parallel toward the downstream in the lab tunnel, while for the field tunnel, the diluted exhaust rotates forward due to the effect of the mixing enhancer, illustrated in pathlines in SI Figures S3 and S4.

Of particular note is that in general, the DR characterized in the dilution sampling measurements is the value at the end of the dilution tunnels. However, inside the dilution tunnel (especially near the exhaust pipe inlet), there is a wide range of DRs, due to the spatial inhomogeneity. With LES model, CTAG captures the instantaneously and time-averaged profile of DRs inside the tunnels, which can be a challenge for those models based on empirical equations or assumptions, especially in complicated domains.

In summary, the complexity in the turbulent flow field makes it very beneficial to employ a suitable unsteady turbulence model for predicting the evolution of exhaust particles, as described in Section 5.2.

5.2. Evaluation of Aerosol Dynamics Inside Two Dilution Tunnels. In this section, we describe the profiles of simulated aerosol properties (i.e., nucleation rates and UFP concentrations) and compare the measured and simulated PSDs.

5.2.1. New Particle Formation and the Evolution of Particle Number Concentrations Inside the Tunnels. Figure 3a illustrates the nucleation process in the two dilution tunnels and only the areas near the injection of the exhaust are shown since the nucleation process ceases quickly after the exhaust is diluted. Turbulent mixing affects the local gaseous species concentration, temperature, and *RH*, which play important roles in determining the formation of *UFPs*. The maximum nucleation rate in the lab tunnel *DR20* (Case 1) is approximately 2−3 orders higher than the other three cases (Case 2, 3 and 4). The dilution air in Case 2, 3, and 4 is drier than Case 1, which partially contributes to the differences. Further analysis is conducted in Section 5.3.1.

The contours of UFP concentration inside the dilution tunnels are shown in Figure 3b. The level of UFP concentration varies among cases due to their different nucleation rates. With a stronger nucleation process, the UFP concentration at the end of the lab tunnel DR20 (Case 1) is higher than those in the other three cases (shown in Table 2 as well). The UFP concentration at the end of the lab tunnel under DR120 is similar to that of the field tunnel under DR120 since nucleation is suppressed for both cases. In the area adjacent to the injection of exhaust, turbulence plays a crucial role in mixing the exhaust with the dilution air, and the strength of nucleation dominates the level of UFP concentration. Further downstream, nucleation terminates and the growth of UFPs by condensation and coagulation continues.

5.2.2. Evaluation of PSDs between CTAG and Measurement. The comparisons between the measured and simulated dilution-corrected PSDs (i.e., PSDs at the end of the tunnel multiplied by their corresponding DRs) are shown in Figure 4 for both dilution tunnels under DR20 and DR120 conditions. A large nucleation mode is observed for the lab tunnel under DR20 due to the strong nucleation, while it is not observed for

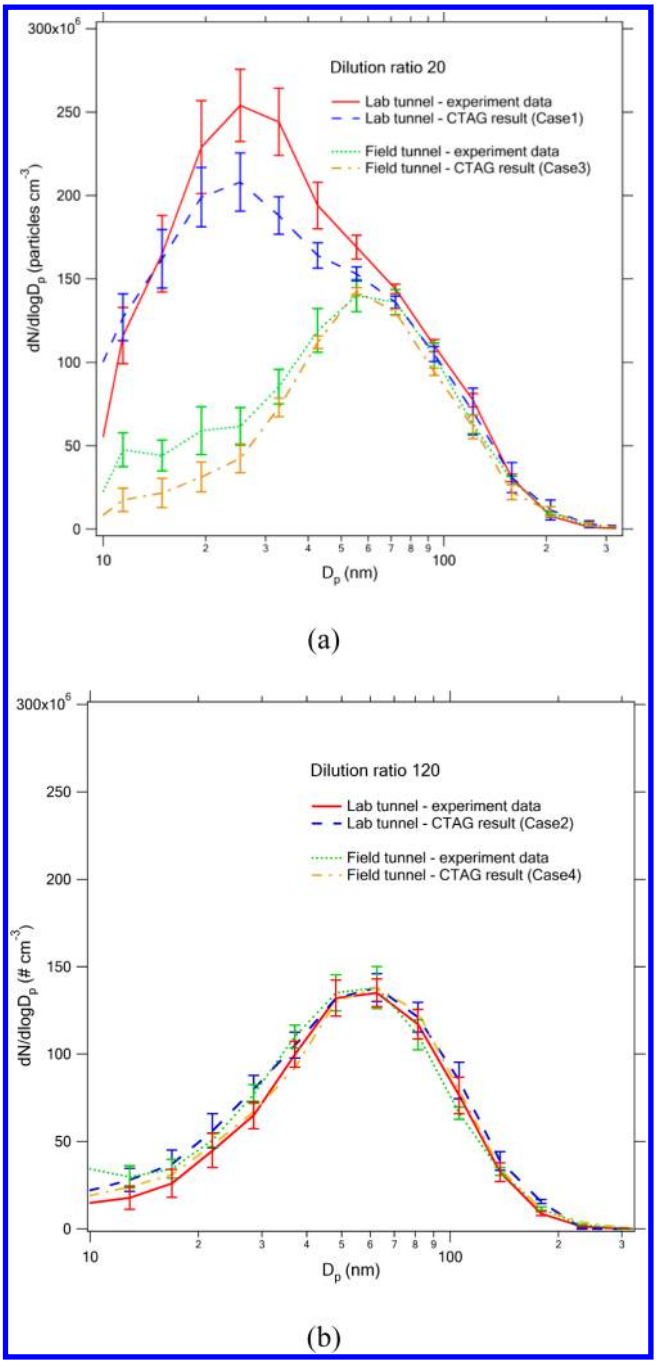

Figure 4. Dilution-corrected PSDs at the end of two dilution tunnels under (a) DR20 and (b) DR120.

the other three cases. Therefore, both measurements and simulations in the study show that nucleation is sensitive to the dilution conditions (e.g., RH of the dilution air and the mixing type). A major portion of the follow-up discussions will be devoted to investigating the origins of the observed discrepancies. Due to the growth by the condensation of OC and sulfuric acid, as well as the coagulation between the particles, the nucleation mode at the end of the lab tunnel at DR20 peaks at around 25 nm. It is also observed that the accumulation mode is relatively stable, which is consistent with the hypothesis that the majority of particles in the accumulation mode are carbonaceous agglomerates that are unaffected by the changes in dilution conditions.[2] Meanwhile, the volume size

dx.doi.org/10.1021/es302376d | *Environ. Sci. Technol.* 2013, 47, 889−898

Table 3. Sensitivity Study of Dilution Parameters (Variations from the Validated Cases Are Highlighted in Bold)

		DR	RH of dilution air (@ 297 K)	mixing enhancer	RT	dilution-corrected UFP concentration at the end of tunnels (particle cm^{-3})	relative change based on Base Case	maximum dilution rate of exhaust (s^{-1})
Case 1[a]	lab tunnel	20	10%	no	~2.5 s	1.54×10^9	N/A (Base Case)	83.2
Case 3	field tunnel	20	<1%	yes	~2.5 s	7.47×10^8	−5.3% (to Case 6)	31.9
Case 5	lab tunnel	20	**<1%**	no	~2.5 s	8.42×10^8	−45.5% (to Case 1)	83.2
Case 6[a]	field tunnel	20	**10%**	yes	~2.5 s	7.89×10^8	N/A (Base Case)	31.9
Case 7	lab tunnel	20	10%	**yes**	~2.5 s	1.82×10^9	18.0% (to Case 1)	124.8
Case 8	field tunnel	20	10%	**no**	~2.5 s	7.76×10^8	−1.6% (to Case 6)	11.9
Case 9	lab tunnel	20	10%	yes	**~1.3 s**	2.22×10^9	43.3% (to Case 1)	160.1
Case 10	lab tunnel	20	10%	no	**~5.0 s**	8.50×10^8	−45.0% (to Case 1)	36.5
Case 11	field tunnel	20	10%	yes	**~1.3 s**	8.22×10^8	4.2% (to Case 6)	49.7
Case 12	field tunnel	20	10%	yes	**~5.0 s**	7.49×10^8	−5.1% (to Case 6)	18.1

[a]Base cases of lab tunnel (Case 1) and field tunnel (Case 6).

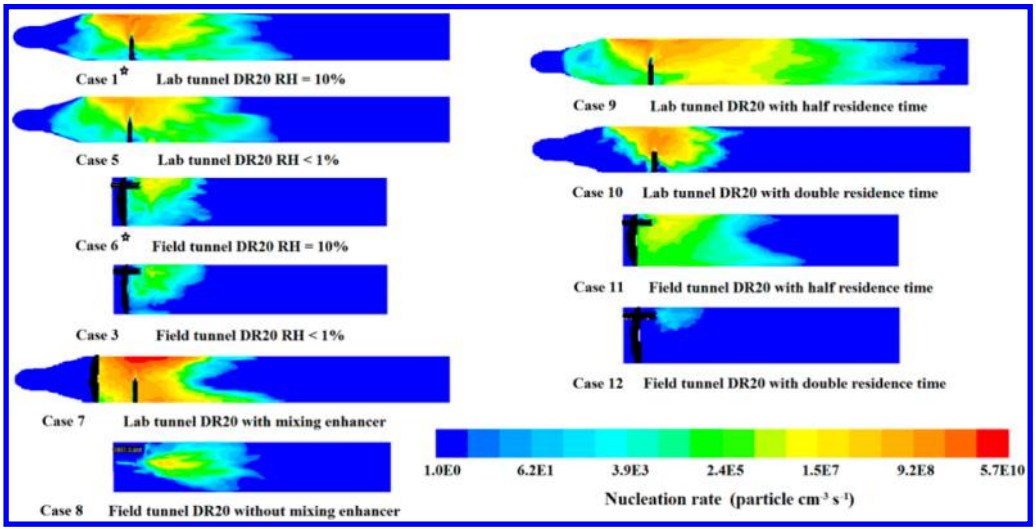

Figure 5. Time-averaged nucleation rate inside two dilution tunnels for sensitivity studies. Case 1 and Case 6 are used as base cases.

distributions from both measurement and CTAG predictions show good agreements for the two dilution tunnels, indicating that the observed new particle formation does not affect the overall mass or the accumulation mode. The volume size distributions are shown in SI Figure S8.

PSDs simulated by CTAG generally capture the general shapes of measured PSDs, although the model under-predicts the concentrations near the peak of the nucleation mode for the lab tunnel under DR20 (Case 1) in Figure 4a. This may be caused by the difference between estimated and actual levels of sulfuric acid, and further analysis is in Section 5.5. The weighted deviation of PSD for the lab tunnel under DR20 between simulation and measurement is 12.6%, while the weighted deviation for the field tunnel under DR20 is 8.5%. The differences between simulation and experiment for both tunnels under DR120 are less than 3% since only the accumulation mode exists.

5.3. Sensitivity Analysis of Dilution Parameters. As discussed earlier, there are three main differences in dilution parameters during the measurements: RH (Group II), the mixing type (Group I), and the mixing enhancer (Group I). Therefore, the method of exclusion with controlled numerical experiments is utilized to investigate their individual effect on the formation of UFPs. The effect of RH (Group II) is studied first, since the consistency in Group II can provide the unbiased conditions for later investigations in Group I in Section 5.3.2 and 5.3.3. DR is fixed as 20 for all cases, while other parameters are shown in Table 3.

5.3.1. Effect of RH of the Dilution Air (Group II). RH of dilution air is found to have a considerable effect on the formation of UFPs during the dilution process, and higher RH can increase the amount of nucleation mode particles.[26] Sensitivity studies (Case 5 and Case 6) are conducted, since RH of the dilution air used in the experiment is different for the two tunnels, which could cause the difference in PSDs.

As shown in Figure 5, for both tunnels, stronger nucleation can be observed under the higher RH, i.e., 10% (Case 1 vs Case 5; Case 3 vs Case 6). Meanwhile, for Case 3 and Case 5, even if the dilution air is dry (<1%), nucleation still occurs in both tunnels. This is because the large amount of water vapor in the exhaust can increase the RH of the mixture to more than 5% rapidly near the exhaust pipe when the hot exhaust is cooled down by the dilution air at room tempeature (shown in SI Figure S7). PSDs in Figure 6a show that a large nucleation mode exists under the high RH for lab tunnel (Case 1), while under the low RH (Case 5), nucleation is considerably suppressed. The UFP concentration at the end of the lab tunnel under low RH is 45.5% lower than that under high RH (Table 3). For the field tunnel, RH has shown a smaller impact on nucleation and there is no nucleation mode observed under both high and low RH (Case 3 and Case 6). The difference in UFP concentration is only 5.3%.

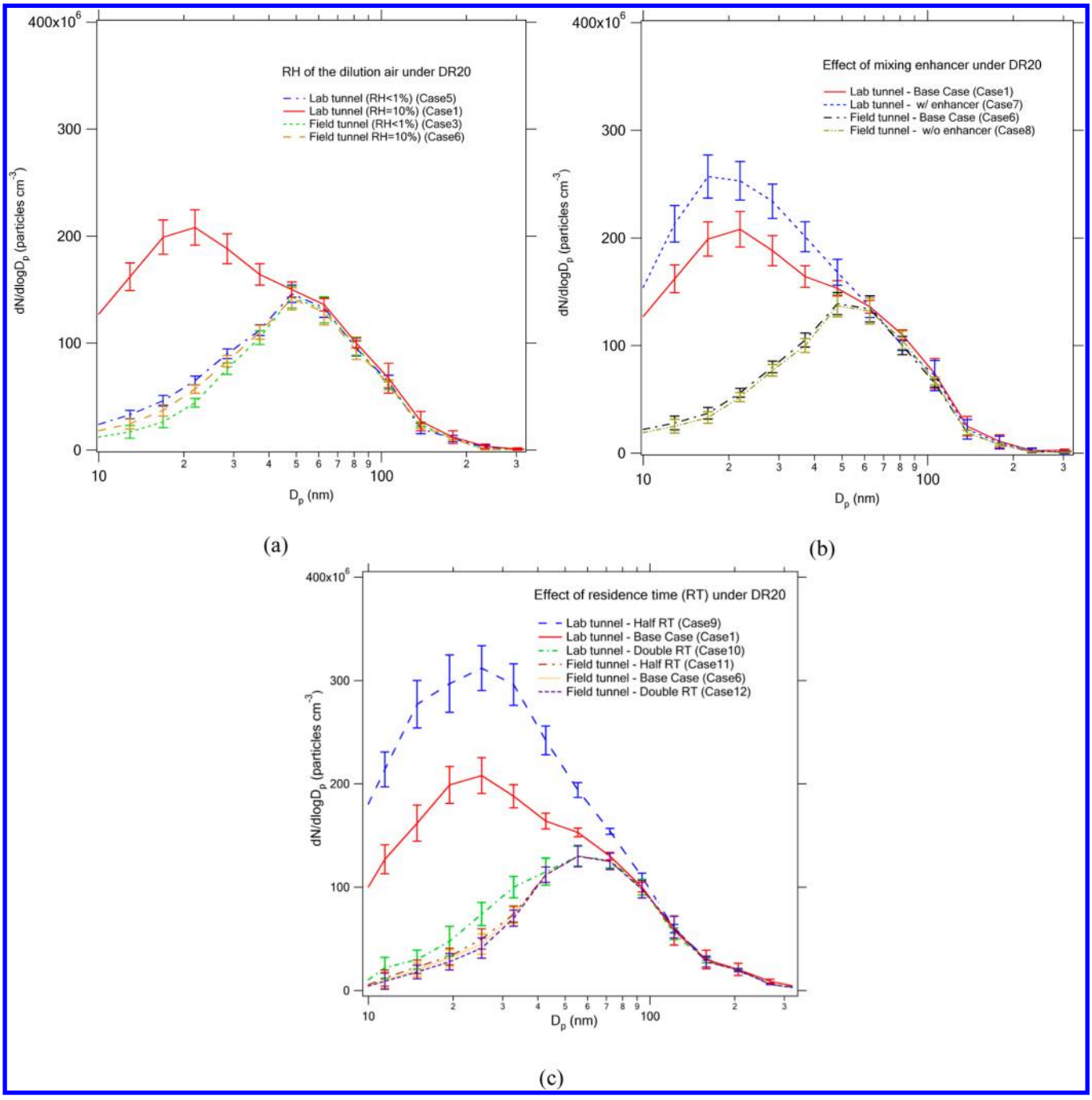

Figure 6. Dilution-corrected PSDs at the end of the two dilution tunnels for sensitivity studies.

The intercomparison shows that under the same RH of 10%, the UFP concentration in the lab tunnel is still about 95.2% higher than that in the field tunnel. Therefore, RH cannot explain the difference between the two dilution tunnels for the nucleation event, and in the following studies, Case 1 and Case 6 (with the same RH of 10%) serve as the base cases for the lab tunnel and field tunnel, respectively.

5.3.2. Effect of the Mixing Types and Mixing Enhancer (Fixed Parameter in Group I). As discussed earlier, there are two main differences in the configurations of the two dilution tunnels, one is the mixing type, and the other is the mixing enhancer. Since the mixing type is the basic design of the dilution tunnel and remains unchanged, sensitivity study regarding the installation or not of the mixing enhancer is then conducted (Case 7 and Case 8), while other parameters in Group I and II are the same for both tunnels.

Lab Tunnel Installed with the Mixing Enhancer. For comparison, the same fan-shaped mixing enhancer is installed in lab tunnel upstream where the dilution air and exhaust meet, as shown in Figure 5 (Case 7). The mixing enhancer disturbs the dilution air before it mixes with exhaust, and increases the turbulence level of the incoming dilution air. As shown in Figure 5, the mixing enhancer becomes a distinct boundary for the nucleation process since the mixing of exhaust and dilution air occurs instantaneously behind the mixing enhancer. As illustrated in Figure 5, the maximum nucleation rate is enhanced with the mixing enhancer (Case 7 vs Case 1), while a larger nucleation mode exists in the PSD of lab tunnel

dx.doi.org/10.1021/es302376d | Environ. Sci. Technol. 2013, 47, 889−898

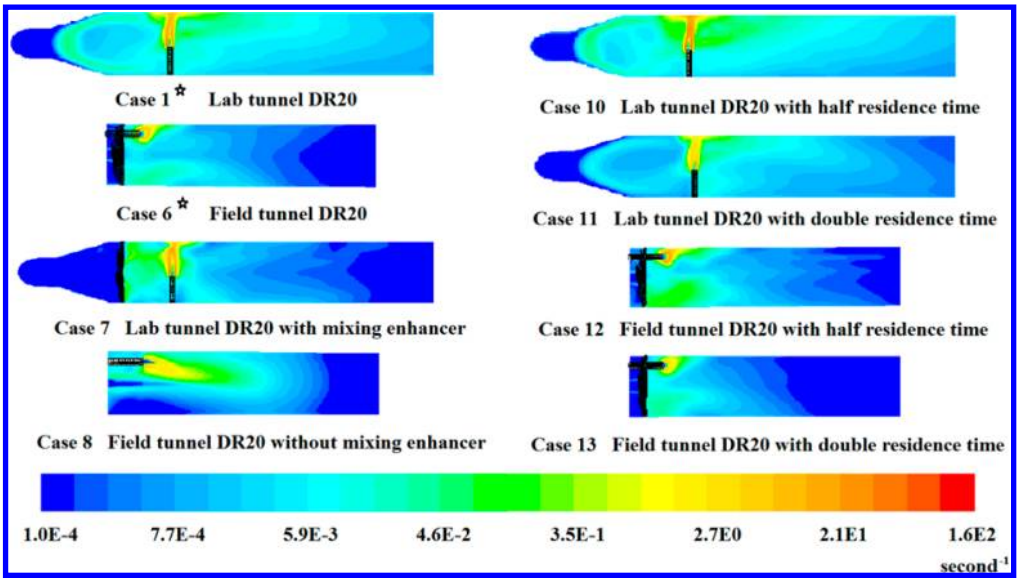

Figure 7. Time-averaged dilution rate of exhaust inside the dilution tunnels.

with the mixing enhancer (Figure 6b). The UFP concentration at the end of lab tunnel increases 18.0% when compared to the case without the mixing enhancer (Case 1).

Field Tunnel without Mixing Enhancer. The field tunnel without the mixing enhancer is also created to investigate the effect of the mixing enhancer inside field tunnel (Case 8). As shown in Figure 5, since there is no disturbance from the mixing enhancer, nucleation occurs at the shear layer where the exhaust encounters the dilution air. The maximum nucleation rate is similar to that of field tunnel with mixing enhancer. PSDs in Figure 6b have shown little difference for the cases with or without the mixing enhancer in field tunnel. The UFP concentration at the end of the field tunnel for the case without the enhancer is only 1.6% lower than that with the enhancer (Table 3), suggesting that, under the coaxial mixing, the mixing enhancer plays a less important role in altering the nucleation process.

For both tunnels without the mixing enhancer (Case 1 and Case 8), the UFP concentration at the end of the lab tunnel is 98.5% higher than that of the field tunnel, suggesting that instead of the mixing enhancer, the mixing type causes the main difference in the formation of UFPs between the two dilution tunnels.

5.3.3. Effect of Residence Time (RT) Inside the Dilution Tunnel (Variable Parameter in Group I). Besides the investigations on the differences between the two dilution tunnels, the effect of RT is also studied. RT affects the flow and mixing profiles inside the dilution tunnels. RT can be altered when the flow rates of exhaust and dilution air vary at the same ratio simultaneously. Two RTs (~1.3 s and ~5.0 s) are generated for the comparisons (Cases 9 to 12).

As shown in Figure 5, the levels of nucleation have shown large differences under various RTs, even within the same tunnel. For both tunnels, stronger nucleation can be observed under the shorter RT. A similar trend can be found for the PSDs at the end of the dilution tunnels under various RTs, as illustrated in Figure 6c. It is shown that for the lab tunnel, the nucleation mode varies more significantly than that for the field tunnel. The differences in the UFP concentrations can vary by up to 45% with various RT for the lab tunnel and ~5% for the field tunnel (Table 3), suggesting the importance of RT in the operation of different types of dilution tunnels. Meanwhile, sensitivity studies of the coagulation process have been conducted under different RTs inside the dilution tunnels. It is found that, besides a weaker nucleation, the coagulation process under a longer RT (~5.0 s) is also important for the change in the particle number concentrations (e.g., ~9.7% decrease in lab tunnel), while coagulation plays a smaller role in determining the number concentration under a short RT (~1.3 s) (e.g., ~3.4% decrease in lab tunnel).

5.4. Dilution Rate of the Exhaust, a Potential Unifying Parameter. In the sensitivity study, it has been shown that even under the same mixture properties (Group II), there are still large differences in the formation of UFPs. Therefore, aerodynamics (Group I) is responsible for the differences in nucleation. Aerodynamics affects the mixing characteristics of exhaust and dilution air, which can change the local supersaturation of the diluted exhaust. So far, there is not a defined set of parameters to characterize the aerodynamics. As a preliminary study, the dilution rate (or the mixing rate) of the exhaust is introduced to characterize the effect of aerodynamics on the dilution process and is represented by the scalar dissipation rate of exhaust.[27,28] The scalar dissipation rate computes the rate at which the diesel exhaust and dilution air are brought together at the molecular level.

$$\varepsilon_{\tilde{\xi}} = C_{\phi}\langle\xi'^2\rangle\frac{\varepsilon}{k} \quad (1)$$

where k and ε are the turbulent kinetic energy and turbulent dissipation rate, respectively. $\langle\xi'^2\rangle$ is the mixture variance, where "mixture" represents the diluted exhaust. C_{ϕ} equals 2.0.[28]

The contour of dilution rate and the maximum values for various cases are shown in Figure 7 and Table 3. It can be seen that the level of dilution rate varies significantly with the mixing type, the mixing enhancer, and RT. T-mixing in lab tunnel has the advantage of allowing a higher degree of penetration into the cross-stream than the coaxial mixing in the field tunnel (Case 1 vs Case 6). The corresponding maximum dilution rate in the lab tunnel (83.2 s^{-1}) is higher than that in the field tunnel (31.9 s^{-1}). The mixing enhancer also tends to increase the dilution rate, especially in areas directly behind the mixing enhancer (Case 1 vs Case 7), which prompts the formation of

dx.doi.org/10.1021/es302376d | Environ. Sci. Technol. 2013, 47, 889−898

UFPs. Furthermore, RT can affect the level of dilution rate significantly. For the lab tunnel, the maximum dilution rate increases 92.4% under the half RT and decreases 56.1% with the double RT. A similar trend can also be found for the field tunnel. In general, the dilution rate of exhaust is mainly related to the aerodynamics (Group I).

A previous study finds that the possibility of nucleation could become higher with a shorter dilution time duration, which demonstrates that extremely rapid dilution is crucial for obtaining supersaturation where nucleation is possible.[29] This effectively interprets our experimental and simulation results, and illustrates that the dilution rate of exhaust can affect the local saturation ratio and alter the formation of UFPs. A similar trend can also be found in other types of nucleation, e.g., Moody and Collins[30] show that increasing the rate of mixing also increases the rate of formation of TiO_2 particles. Since the dilution process is conducted under a highly turbulent environment, the dilution rate of exhaust is positively related to the level of turbulence, as illustrated in SI Figure S9.

5.5. Uncertainty and Limitation. There are still a number of uncertainties in some input parameters that were not measured directly, e.g., the sulfuric acid concentration in the exhaust, which is a critical parameter for nucleation. The level of sulfuric acid is dependent on what fraction of the SO_2 formed in the engine is oxidized to SO_3, i.e., cr,[1] and is difficult to measure directly. In the simulation of aerosol dynamics, uncertainty rises during the selection of cr, as 4−8% is used in the study of Vouitsis et al.,[13] while cr can be much larger if aftertreatment devices are installed (e.g., diesel oxidation catalyst (DOC), diesel particulate filter (DPF)). There is also a potential contribution from the sulfur in the lubricant oil, especially when ultralow sulfur fuels are used.[13,31] Sensitivity studies of the selection of cr are conducted and discussed in the SI.

The CTAG model still needs further improvement, e.g., the binary homogeneous nucleation model of water−sulfuric acid vapor is used to capture the formation of UFPs.[32] However, there might be other types of nucleation (e.g., nucleation of organics) occurring during the dilution process.[6]

The CTAG model is currently computationally expensive for operational purposes. However, it can become a crucial tool for the understanding of the aerosol dynamics in a highly turbulent environment inside dilution tunnels and help improving the measurements of particulate emissions.

6. IMPLICATIONS

We have investigated the effects of aerodynamics-related parameters and mixture properties-related parameters on the evolution of exhaust particles during the dilution process inside two dilution tunnels. The dilution rate of exhaust was identified as a potentially unifying parameter describing aerodynamics. In general, the formation of new particles increases with the increasing dilution rate of exhaust. Through the comparison, we find that the lab tunnel shows the tendency to capture the atmospheric dilution with a strong nucleation mode, while the field tunnel might be used to preserve the exhaust properties as observed inside the exhaust pipe. However, further investigations are needed, especially comparing the results from the dilution tunnels with those from atmospheric dilution on the roadways.

Our study suggests the benefits of simulation tools such as CTAG on improving the design and operation of the dilution tunnels. Simulation-aided designs may become effective in reducing the costs of conducting emission measurements. Many parameters can be varied during dilution tunnel operations to alter the turbulent flow field and affect the aerosol dynamics. With mechanistic understandings of the coupled turbulence and aerosol dynamic processes, we can design and operate the dilution systems to achieve the different goals, e.g., retaining tailpipe-level emissions or capturing the effects of plume processing on exhaust particles.[2]

■ ASSOCIATED CONTENT

Supporting Information

Additional text, figures, and tables as mentioned in the text. This material is available free of charge via the Internet at http://pubs.acs.org.

■ AUTHOR INFORMATION

Corresponding Author

*Phone: 607-254-5402; e-mail: kz33@cornell.edu.

Notes

The authors declare no competing financial interest.

■ ACKNOWLEDGMENTS

We acknowledge the U.S. Environmental Protection Agency (USEPA) and California Air Resources Board (CARB) for the funding support. K.M.Z. would also like to acknowledge the support from an ORISE fellowship. We also thank Drs. Prakash Bhave, Kathleen Fahey, Havala Olson Taylor Pye at USEPA, and Dr. Satbir Singh at Carnegie Mellon University for the valuable discussions and suggestions. Although the research described in this article has been partially funded by USEPA grant R834561, it has not been subject to the Agency's review and therefore does not necessarily reflect the views of the Agency, and no official endorsement should be inferred.

■ REFERENCES

(1) Burtscher, H. Physical characterization of particulate emissions from diesel engines: A review. *J. Aerosol Sci.* **2005**, *36* (7), 896−932.

(2) Lipsky, E. M.; Robinson, A. L. Design and evaluation of a portable dilution sampling system for measuring fine particle emissions from combustion systems. *Aerosol Sci. Technol.* **2005**, *39* (6), 542−553.

(3) Brockmann, J. E.; Liu, B. Y. H.; McMurry, P. H. A sample extraction diluter for ultrafine aerosol sampling. *Aerosol Sci. Technol.* **1984**, *3* (4), 441−451.

(4) Hildemann, L. M.; Cass, G. R.; Markowski, G. R. A dilution stack sampler for collection of organic aerosol emissions: Design, characterization and field tests. *Aerosol Sci. Technol.* **1989**, *10* (1), 193−204.

(5) Lyyranen, J.; Jokiniemi, J.; Kauppinen, E. I.; Backman, U.; Vesala, H. Comparison of different dilution methods for measuring diesel particle emissions. *Aerosol Sci. Technol.* **2004**, *38*, 12−23.

(6) Ronkko, T.; Virtanen, A.; Vaaraslahti, K.; Keskinen, J.; Pirjola, L.; Lappi, M. Effect of dilution conditions and driving parameters on nucleation mode particles in diesel exhaust: Laboratory and on-road study. *Atmos. Environ.* **2006**, *40* (16), 2893−2901.

(7) Strand, M.; Bohgard, M.; Swietlicki, E.; Gharibi, A.; Sanati, M. Laboratory and field test of a sampling method for characterization of combustion aerosols at high temperatures. *Aerosol Sci. Technol.* **2004**, *38*, 757−765.

(8) Abdul-Khalek, I.; Kittelson, D.; Brear, F. *The Influence of Dilution Conditions on Diesel Exhaust Particle Size Distribution Measurements*; SAE Technical Paper 1999-01-1142; 1999, 10.4271/1999-01-1142.

(9) Shi, J. P.; Harrison, R. M. Investigation of ultrafine particle formation during diesel exhaust dilution. *Environ. Sci. Technol.* **1999**, *33*, 3730−3736.

(10) Casati, R.; Scheer, V.; Vogt, R.; Benter, T. Measurement of nucleation and soot mode particle emission from a diesel passenger car

in real world and laboratory in situ dilution. *Atmos. Environ.* **2007**, *41* (10), 2125−2135.
(11) Lipsky, E.; Stanier, C. O.; Pandis, S. N.; Robinson, A. L. Effects of sampling conditions on the size distribution of fine particulate matter emitted from a pilot-scale pulverized-coal combustor. *Energy Fuels* **2002**, *16* (2), 302−310.
(12) Pyykonen, J.; Miettinen, M.; Sippula, O.; Leskinen, A.; Raunemaa, T.; Jokiniemi, J. Nucleation in a perforated tube diluter. *J Aerosol Sci.* **2007**, *38*, 172−191.
(13) Vouitsis, E.; Ntziachristos, L.; Samaras, Z. Modelling of diesel exhaust aerosol during laboratory sampling. *Atmos. Environ.* **2005**, *39* (7), 1335−1345.
(14) Wang, Y. J.; Zhang, K. M. Coupled turbulence and aerosol dynamics modeling of vehicle exhaust plumes using the CTAG model. *Atmos. Environ.* **2012**, *59*, 284−293.
(15) Kittelson, D.; Arnold, M.; Watts, W. F. *Review of Diesel Particulate Matter Sampling Methods, Supplemental Report # 2, Aerosol Dynamics, Laboratory and On-Road Studies*; University of Minnesota: Minneapolis, MN, 1998
(16) Mathis, U.; Ristimaki, J.; Mohr, M.; Keskinen, J.; Ntziachristo, L.; Samaras, Z.; Mikkanen, P. Sampling conditions for the measurement of nucleation mode particles in the exhaust of a diesel vehicle. *Aerosol Sci. Technol.* **2004**, *38*, 1149−1160.
(17) Khalek, I. A.; Spears, M.; Charmley, W. *Particle Size Distribution from a Heavy-Duty Diesel Engine: Steady-State and Transient Emission Measurement Using Two Dilution Systems and Two Fuels*; SAE Paper 2003-01-0285; 2003, 10.4271/2003-01-0285.
(18) Maricq, M. M.; Chase, R. E.; Podsiadlik, D. H.; Vogt, R. *Vehicle Exhaust Particle Size Distributions: A Comparison of Tailpipe and Dilution Tunnel Measurements*; SAE Paper 1999-01-1461; 1999, 10.4271/1999-01-1461.
(19) Carpentieri, M.; Kumar, P. Ground-fixed and on-board measurements of nanoparticles in the wake of a moving vehicle. *Atmos. Environ.* **2011**, *45*, 5837−5852.
(20) Wehner, B.; Uhrner, U.; Von Löwis, S.; Zallinger, M.; Wiedensohler, A. Aerosol number size distributions within the exhaust plume of a diesel and a gasoline passenger car under on-road conditions and determination of emission factors. *Atmos. Environ.* **2009**, *43* (6), 1235−1245.
(21) *ANSYS FLUENT 12.1 User's Guide*; ANSYS, 2010.
(22) Guleren, K. M.; Turan, A. Validation of large-eddy simulation of strongly curved stationary and rotating U-duct flows. *Int. J. Heat Fluid Flow* **2007**, *28*, 909−921.
(23) Wegner, B.; Huai, Y.; Sadiki, A. Comparative study of turbulent mixing in jet in cross-flow configurations using LES. *Int. J. Heat Fluid Flow* **2004**, *25*, 767−775.
(24) Fox, R. O. *Computational Models for Turbulent Reacting Flows*; Cambridge University Press, 2003, Chapter 5.10.
(25) Subramanian, R.; Khlystov, A. Y.; Cabada, J. C.; Robinson, A. L. Positive and negative artifacts in particulate organic carbon measurements with denuded and undenuded sampler configurations. *Aerosol Sci. Technol.* **2004**, *38*, 27−48.
(26) European Commission. *Particulates. Characterization of Exhaust Particulate Emissions from Road Vehicles*; 2005.
(27) Bray, K. N. C. Turbulent flows with premixed reactants. *Top. Appl. Phys.* **1980**, *44*, 115−183.
(28) Pope, S. B. PDF methods for turbulent reacting flows. *Prog. Energy Combust. Sci.* **1985**, *11*, 119−192.
(29) Zhang, K. M.; Wexler, A. S. Evolution of particle number distribution near roadways - Part I: analysis of aerosol dynamics and its implications for engine emission measurement. *Atmos. Environ.* **2004**, *38* (38), 6643−6653.
(30) Moody, E. G.; Collins, L. R. Effect of mixing on the nucleation and growth of titania particles. *Aerosol Sci. Technol.* **2003**, *37*, 403−424.
(31) Herner, J. D.; Hu, S.; Robertson, W. H.; Huai, T.; Chang, M.-C. O.; Rieger, P.; Ayala, A. Effect of advanced aftertreatment for PM and NO_x reduction on heavy-duty diesel engine ultrafine particle emissions. *Environ. Sci. Technol.* **2011**, *45*, 2413−2419.
(32) Vehkamaki, H.; Kulmala, M.; Lehtinen, K. E. J. Modelling binary homogeneous nucleation of water-sulfuric acid vapors: Parameterization for high temperature emissions. *Environ. Sci. Technol.* **2003**, *37* (15), 3392−3398.
(33) Grieshop, A. P.; Miracolo, M. A.; Donahue, N. M.; Robinson, A. L. Constraining the Volatility Distribution and Gas-Particle Partitioning of Combustion Aerosols Using Isothermal Dilution and Thermodenuder Measurements. *Environ. Sci. Technol.* **2009**, *43* (13), 4750−4756.